Hindawi
Journal of Spectroscopy
Volume 2019, Article ID 9326789, 13 pages
https://doi.org/10.1155/2019/9326789

Research Article

Study on the Processing Technology of Calamine Calcination by Near-Infrared Spectroscopy

Xiaodong Zhang[1], **Long Chen**[2], **Yu Bai**[3] **and Keli Chen**[1]

[1]*Key Laboratory of Ministry of Education on Traditional Chinese Medicine Resource and Compound Prescription & Hubei University of Chinese Medicine, Wuhan 430065, China*
[2]*Xiangyang Central Hospital, Xiangyang, Hubei 441500, China*
[3]*Mayinglong Pharmaceutical Group Co., Wuhan 430065, China*

Correspondence should be addressed to Keli Chen; kelichen@126.com

Received 5 November 2018; Revised 25 January 2019; Accepted 14 February 2019; Published 10 March 2019

Academic Editor: Feride Severcan

Near-infrared spectroscopy has been widely used in qualitative and quantitative analysis and online monitoring in the production process of traditional Chinese medicines. The aim was to establish a fast determination model of zinc oxide (ZnO) content in calcined calamine and to explore methods through judging the end point of calamine calcination. Eight batches of calamine samples sourced from hydrozincite with different sizes and textures were calcined at different temperatures. During the calcination process, ZnO contents, X-ray diffraction (XRD) patterns, and near-infrared spectra of the samples were used to analyze their changes rules. The model of determining ZnO content of calcined calamine was established to use near-infrared spectroscopy based on the partial least squares (PLS) regression algorithm. In addition, this paper summarized the change rules of calamine in calcination according to XRD patterns, using the "K value" quantitative method to define the characteristic T value. When the T value was equal to 1.00 (100%), that is to say, the calamine sample was completely calcined. Then, matching the near-infrared spectroscopy data with the T value and establishing the T value analysis model using the PLS algorithm were performed. Through cross and independent validation and evaluation, it was proved that the two models were very effective and had strong predictive abilities. Finally, the purpose of the online monitoring of the calcination process and controlling the quality of the calcined calamine was achieved.

1. Introduction

Calamine, a common mineral used in Chinese Medicine and recorded in China Pharmacopoeia (ChP, the 2015 Edition Volume I), is smithsonite belonging to carbonate minerals in the calcite group and mainly contains zinc carbonate ($ZnCO_3$) [1]. However, according to literature reports and findings in our investigations, calamine is also sourced from hydrozincite [$Zn_5(CO_3)_2(OH)_6$] and the latter is the current mainstream of commercial calamine in the market [2–4]. Calamine must be calcined before being used as a drug. The calcined calamine has the actions to counteract toxicity, to clear the eye off corneal opacity and to relieve itching [1]. It is commonly used in the treatment of eye, skin, anorectal diseases, for example, Musk hemorrhoids ointment for treating hemorrhoids and calamine lotion for relieving itching. The study has shown that the calcination process is the decomposition of $ZnCO_3$ or $Zn_5(CO_3)_2(OH)_6$ into the active ingredient ZnO [5]. The ChP stipulates that the ZnO content of calcined calamine should not be less than 56% [1]. However, in the actual calcination process, if the calamine is not calcined completely, the ZnO content titrated with ethylene diamine tetraacetic acid (EDTA) according to the ChP is actually the total amount of zinc ions in the sample solution, and the obtained result may still comply with the pharmacopoeia. Calamine, if not being completely calcined,

used as a drug not only affects the efficacy but also causes waste of resources.

At present, judging whether calamine is completely calcined is mainly through analysis of X-ray diffraction (XRD) patterns before and after calcination [6]. If the phase analysis of the XRD pattern before calcination shows smithsonite or hydrozincite, and after calcination, the smithsonite or hydrozincite phase in the XRD pattern disappeared and produced the ZnO phase, that is to say, the calamine is completely calcined. Although the XRD analysis method is accurate and reliable, the analysis cost is high and online detection cannot be realized in the production process. In addition, since most of the collected calamine samples are sourced from hydrozincite [3, 4], this study aims to explore new methods for judging the calcination end point of the calamine sourced from hydrozincite.

Near-infrared (NIR) spectra are the results of light absorption by organic molecules in the spectral region of 780–2500 nm [7]. Characteristic bands are produced in the NIR spectra of minerals by interaction of electromagnetic radiation with the atoms and molecules that are present in these minerals as a result of electronic and vibrational spectroscopic processes [8, 9]. As a fast, simple, nonpolluting, nondestructive, portable, and on the site analytical technique, NIR spectroscopy has been widely used in the qualitative identification, quantitative analysis, online monitoring, and drug supervision of traditional Chinese medicines [10–13].

In this study, simulated near-infrared spectroscopy online monitoring of calamine calcination process was performed. The change rules of ZnO contents were summarized according to XRD patterns and NIR spectra in the process of calamine calcination. A rapid determination model of ZnO content of calcined calamine was established using near-infrared spectroscopy based on the partial least squares (PLS) algorithm [14]. A method of combining near-infrared spectroscopy with the XRD pattern was also explored to determine whether calamine was completely calcined.

2. Materials and Methods

2.1. Instruments and Software. The instruments and software used for this project consisted of an XPertPro X-ray diffraction instrument (PANalytical Company), a Matrix-F Fourier diffuse reflectance near-infrared spectrometer (Bruker) with sample testing accessories integrated with a fiberoptics probe, an InGaAs detector (Bruker), OPUS 7.5 spectrum analysis software (Bruker), and MDI Jade 6.0 digital signal processing technique software (Materials Data, Inc.).

2.2. Samples. Twenty-eight batches of calamine samples were collected from the Chinese medicine markets, 6 batches of calamine samples were provided by Mayinglong Pharmaceutical Group Co., 18 batches of calamine samples were collected from the Chinese mining areas of Hunan, Guangxi, Guizhou, Yunan, and Sichuan province. A total of 52 batches of calamine samples were obtained [3, 4], and all samples were identified by XRD and the chemical method in the ChP 2015 [1]. Of which, 8 batches of calamine samples were randomly selected, as shown in Table 1.

2.3. Calamine Calcination Process Research

2.3.1. Comparison of XRD Patterns of Calamine before and after Complete Calcination. About 3 g of S1–S6 samples was taken in the crucible, placed within the muffle furnace at 300°C for 100 min; about 3 g of S7-S8 samples were taken in the crucible, placed within the muffle furnace at 400°C for 100 min. Then, all samples were taken out, crashed into powder, and passed through a 200-mesh sieve. Pressed the powder into the groove of the sample plate with a glass plate and collected the XRD pattern according to the instrument operation procedure. XRD patterns were recorded between 3 and 65° (2θ) at a speed of 8 min^{-1}, using a RigakuD/max-1200 diffractometer with CuKα radiation (40 kV, 40 mA).

2.3.2. Variation of ZnO Content and XRD Characteristic T Value. Take out 12 parts from each calamine sample in Table 1 separately, with each part about 3 g. The first part of each sample was taken for calcination for 0 min, and the remaining 11 parts were put into a muffle furnace and then taken out at different calcination time periods. The twentieth parts of the samples were taken out after being calcined for 100 min. For samples S1–S6, calcination temperature was at 300°C. From samples S1, S2, and S4, take out one part every 6 min. From S3 and S5, take out one part every 3 min, and from S6, every 2 min. For sample S7-S8, calcination temperature was at 400°C, and one part was taken out every 2 min. The every part of each sample taken out was cooled and passed through a 200-mesh sieve and then used to determine the ZnO content according to ChP 2015 and collect the XRD patterns and near-infrared spectra.

XRD can be used for quantitative analysis because the intensity of the diffraction peak increases with the content of the phase. However, since the absorption coefficient of different phases is different, the diffraction intensity is not strictly proportional to the content of each phase, so it needs to be corrected [15]. Since 1978, the RIR value, which is the K value, has been added to the PDF card published on the ICDD. It is the ratio of the integrated intensity of the strongest peak of the measured sample to the intensity of the strongest peak of corundum (Al_2O_3) measured by mixing the mass of the sample with Al_2O_3 at a ratio of 1 : 1. It can be written as $K^A_{Al_2O_3} = K^A/K^{Al_2O_3} = I_A/I_{Al_2O_3}$, called the K value of the sample in A phase when corundum is the internal standard. If there are A, B, and C phases in a sample, we can use the A phase as the standard sample, find the RIR value of each phase through the PDF card, and calculate the K value of each phase in the sample, namely,

Table 1: Sample information.

Serial number	Source	Characteristics	Chemical precipitation	Phase composition	ZnO (%)	Test result
S1	Yunan	Around 1 cm, incanus, hard	White	Hydrozincite, hemimorphite	66.57	Authentic
S2	Anguo	Around 1 cm, light pink, hard	White	Hydrozincite	69.59	Authentic
S3	Sichuan	Around 1 cm, light pink, soft	White	Hydrozincite, hemimorphite, dolomite	51.57	Authentic
S4	Guangxi	0.3~1.5 cm, incanus, hard	White	Hydrozincite, hemimorphite, dolomite	43.21	Authentic
S5	Guizhou	Around 0.2 cm, light pink, soft	White	Hydrozincite, hemimorphite, dolomite, calcite	38.12	Authentic
S6	Hunan	Around 0.3 cm, light pink, hard	White, blue	Hydrozincite	67.79	Authentic
S7	Guizhou	Around 1 cm, light pink, soft	White	Hydrozincite, hemimorphite, dolomite, calcite	55.92	Authentic
S8	Yunan	Around 1 cm, incanus, hard	White	Hydrozincite, hemimorphite	64.88	Authentic

$$K_A^A = \frac{K_{Al_2O_3}^A}{K_{Al_2O_3}^A},$$
$$K_A^B = \frac{K_{Al_2O_3}^B}{K_{Al_2O_3}^A}, \quad (1)$$
$$K_A^C = \frac{K_{Al_2O_3}^C}{K_{Al_2O_3}^A}.$$

If there are N phases in a system, the mass fraction of the X phase is

$$W_X = \frac{I_X}{K_A^X \Sigma_{i=A}^N I_i / K_A^i}, \quad (2)$$

where A can be any phase of the selected samples, I_i indicates the integrated intensity of the strongest peak of any phase, $i = A \ldots N$ indicates N phases in the sample.

Therefore, the XRD pattern of the calamine calcination process was analyzed by phase analysis to find the RIR value on the PDF card corresponding to hydrozincite and ZnO, the mass fraction of which can be calculated by equation (1). In order to more intuitively describe the trend of hydrozincite changing over time during calamine calcinations, it is defined that

$$T = \frac{W_{ZnO}}{W_{ZnO} + W_{Zn_5(CO_3)_2(OH)_6}}. \quad (3)$$

Substitute equation (1) into equation (2) to get

$$T = \frac{I_{Zno} RIR_{Zn_5(CO_3)_2(OH)_6}}{I_{Zno} RIR_{Zn_5(CO_3)_2(OH)_6} + I_{Zn_5(CO_3)_2(OH)_6} RIR_{Zno}}, \quad (4)$$

where the corresponding PDF card of ZnO is 75–0576 and the RIR value is 5.53; the corresponding PDF card of $Zn_5(CO_3)_2(OH)_6$ is 75–1100, and the RIR value is 2.49.

Obviously, the range of T value is [0, 1]. When T value is 0, $Zn_5(CO_3)_2(OH)_6$ is not decomposed; when T value is at (0,1), part of $Zn_5(CO_3)_2(OH)_6$ is decomposed into ZnO; when T value is 1, $Zn_5(CO_3)_2(OH)_6$ is completely decomposed into ZnO, that is, the hydrozincite is completely calcined.

2.3.3. Near-Infrared Spectra Collection. Spectra were obtained from 12,500–4,000 cm^{-1} (800–2500 nm) by the coaddition of 32 scans at a resolution of 8 cm^{-1}. Each sample was scanned three times, and the average value of three spectra was used as the spectrum information for analyzing.

2.4. Determination of ZnO Content of Calcined Calamine Using NIRS Based on PLS Algorithm

2.4.1. Modeled Samples and Division of Sample Sets. Ninety-six batches of calcined calamine prepared in Section 2.3.2 were used as part of the modeled sample. The other part was randomly selected from the remaining 44 batches of collected calamine samples and placed in a muffle furnace at 400°C [16] for 100 min, and near-infrared spectra and zinc oxide contents were obtained according to the above methods. For the sufficient sample size, a total of 130 batches of calcined calamine samples were randomly divided into training set, validation set, and test set.

2.4.2. Selection of Modeling Spectral Bands and Spectral Pretreatment Methods. Although the PLS regression algorithm is a "full-spectrum method," if the modeling spectrum is too wide, it will be affected by additional components or spectral noise in the sample, which will make the model worse. Therefore, the selection of modeling spectral bands is beneficial to improve the model forecast accuracy [17]. In addition, the collected spectrum contains not only its own information but also other irrelevant information and noise, such as electrical noise, sample background, and stray light [18]. So, it is necessary to select the modeling spectral bands and spectral pretreatment methods during modeling.

This experiment used the OPUS 7.5/QUANT-2 quantitative analysis software to automatically optimize the modeling parameters. The modeling spectral bands and the pretreatment methods were combined and optimized to,

respectively, establish quantitative analysis models. Since the near-infrared spectral characteristics of the calamine samples were mainly concentrated in the spectral bands of 7434.3–5781.6, 5445.3–4597, and 4598.2–3998.6 cm^{-1}, the three spectral bands were used as the optimized spectral bands. And, SNV, MSC, FD, SD, FD + SNV, and FD + MSC were selected as the pretreatment methods.

2.4.3. Model Validation and Evaluation. The training set was used to establish the model. The validation set was used to validate the model, of which relative mean square error of validation (RMSEV), coefficient of determination (R^2), and ratio of performance to deviation (RPD) were taken as indexes to guide model optimization process. The test set was used to evaluate the model, of which relative mean square error of prediction (RMSEP), R^2, and RPD were taken as indexes to further evaluate the model prediction ability [19]. The smaller the RMSEV and RMSEP, the bigger the R^2 would be, and thus, the predictive effect of the model would be better. Moreover, three RPD categories were defined to account for the model reliability: excellent models with RPD > 2, fair models with 1.4 < RPD < 2, and unreliable models with RPD < 1.4 [20].

2.4.4. Establishment of Near-Infrared Spectral Analysis Model Using PLS Algorithm to Predict T Value. In Section 2.3.2, it was clear that when the T value of XRD pattern was 1, the calamine was completely calcined. Therefore, match the near-infrared spectroscopy data with the T value, and establish the T-value analysis model using the PLS algorithm. The specific method was as follows.

Sixty-two samples that had been collected for the XRD patterns during the calcination of the above 8 batches of calamine samples were randomly divided into training set and prediction set, including 41 training set samples and 21 predicted set samples. Sample spectrum and corresponding T values were imported into OPUS 7.5/QUANT-2 quantitative analysis software. The modeling spectral bands and pretreatment methods were combined and optimized to, respectively, establish quantitative analysis models. Among them, the three ranges of 7434.3–5781.6, 5445.3–4597, and 4598.2–3998.6 cm^{-1} were selected, and SNV, MSC, FD, SD, FD + SNV, and FD + MSC were selected as the pretreatment methods. For the limited sample size, in the process of establishing the model, internal cross-validation and external validation were used to evaluate the predictive ability of the model. Internal cross-validation adopted the leave-one-out cross-validation, of which relative mean square error of cross-validation (RMSECV), R^2, and RPD were taken as indexes to guide model optimization process. In external validation, RMSEP, R^2, and RPD were taken as indexes to further evaluate the model prediction ability.

3. Results and Discussion

3.1. Comparison of XRD Patterns of Calamine before and after Complete Calcination. The XRD patterns of 8 batches of calamine samples before and after calcination for 100 min are shown in Figure 1. According to Figure 1, the main features of the XRD patterns of the 8 batches of calamine samples before calcination were characterized by all samples and the patterns had the strongest peak at $d = 0.677$ nm, followed by strong peaks at $d = 0.315$, 0.272, and 0.248 nm. The phase retrieval showed that these were characteristic of hydrozincite. In addition, some samples also contained impurities. For example, samples S1, S3, S4, S5, S7, and S8 had strong peaks at $d = 0.654$, 0.541, 0.460, 0.410, 0.330, and 0.306 nm. The phase retrieval showed that these were characteristic of heterogeneous. Samples S3, S4, S5, and S7 had strong peaks at $d = 0.289$, 0.219, and 0.179 nm. The phase retrieval showed that these were characteristic of dolomite. Samples S5 and S7 had strong peaks at $d = 0.286$, 0.304, 0.250, and 0.230 nm. The phase retrieval showed that these were characteristic of calcite. Moreover, phase retrieval of all sample XRD patterns showed no ZnO. After calamine samples were calcined at different temperatures for 100 min, the analysis results of XRD patterns showed that the characteristic peaks of hydrozincite were disappeared while the three strongest peaks were generated at $d = 0.281$, 0.260, and 0.247 nm, which were characteristic of ZnO. It was indicated that the hydrozincite was completely decomposed into ZnO, that is, the above samples were completely calcined. Combined with the characteristics of the sample, it could be obtained that the calamine samples of different sizes, textures, and calcination temperatures could be calcined completely after 100 min. In addition, before and after calcination, the dolomite and calcite peaks still existed in some samples and the relative strength slightly increased, indicating that, under the above calcination conditions, these components did not decompose but the relative content increased. Moreover, if there were heterogeneity in the sample composition, after calcination, the characteristic peaks of the heterogeneous sample were sharper and the dispersion was weakened, indicating that the heterogeneity in the sample after calcination was not decomposed, the relative content was increased, and the crystallinity was enhanced.

3.2. Change of ZnO Content and XRD Characteristic T Value of Calamine Samples during Calcination. The change of ZnO content and XRD characteristic T value of 8 batches of calamine samples during calcination are shown in Figures 2 and 3. From Figure 2, the content of ZnO in the calcination process of calamine increased first with the increase of calcination time and then stabilized at the maximum value. When the ZnO content did not change with time, the calamine was calcined completely, judging that the 8 batches of calamine samples completely calcined at 60, 48, 30, 58, 27, 16, 14, and 18 min. From Figure 3, the T value in the calcination process of calamine was gradually increased from 0 to 1 and then remained unchanged, judging that the 8 batches of calamine samples completely calcined at 60, 48, 30, 60, 27, 25, 14, and 18 min. It was found that the judgment results of S4 and S6 samples had a certain deviation from the actual time according to the change trend of ZnO content. Because the experimental process did not

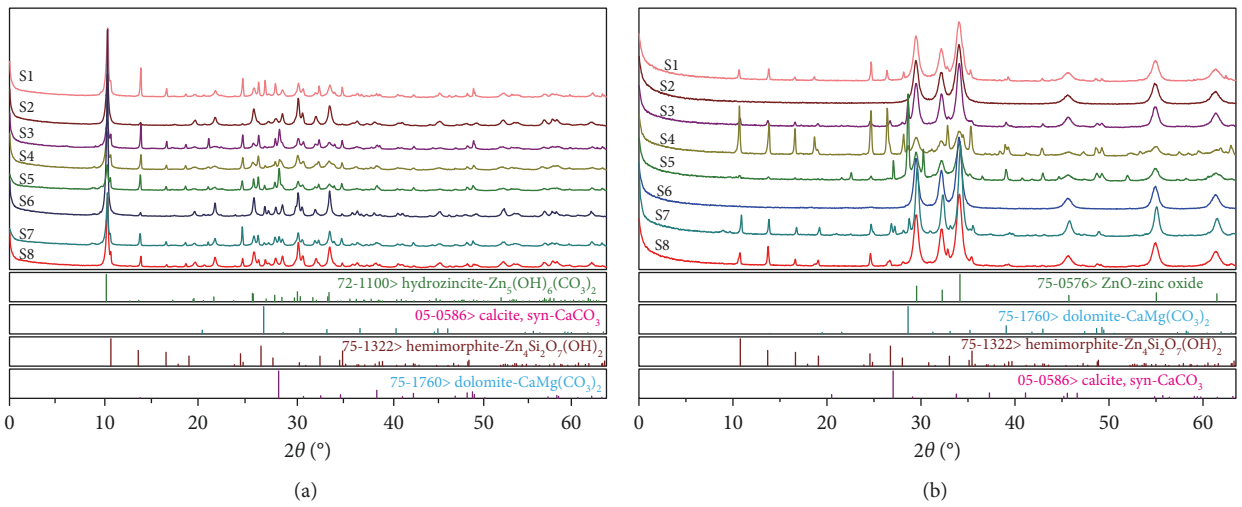

Figure 1: XRD patterns of 8 batches of calamine samples before and after calcination for 100 min.

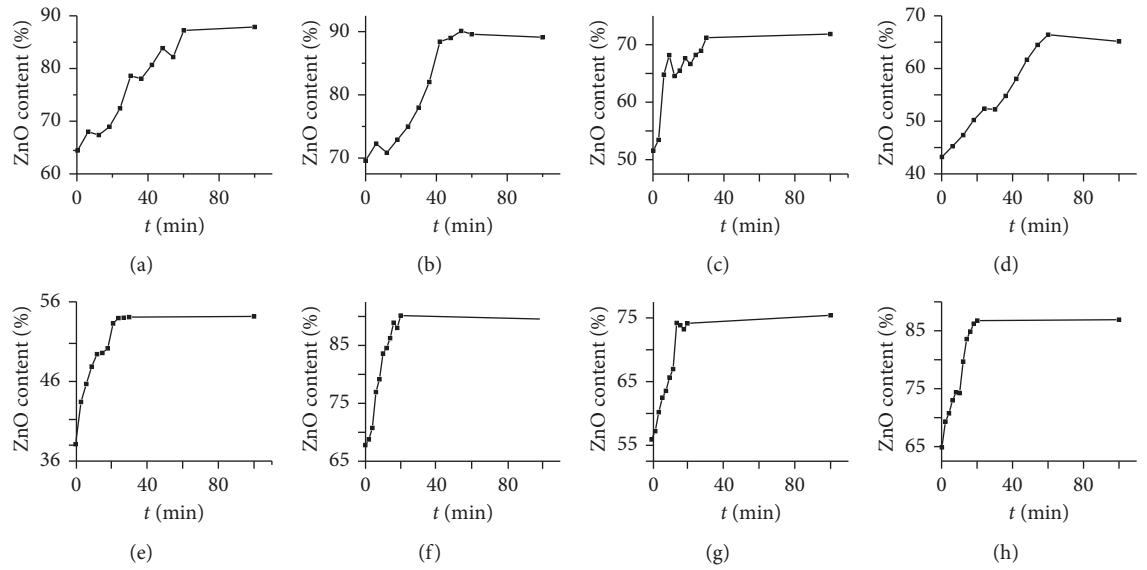

Figure 2: Change of ZnO content of 8 batches of calamine samples during calcination. (a) S1. (b) S2. (c) S3. (d) S4. (e) S5. (f) S6. (g) S7. (h) S8.

guarantee that the content of 12 samples in each batch of samples was consistent, there might be a relatively high or low content of individual samples, and then, there would be small fluctuations in the content of ZnO during calcination, eventually leading to the judgment that the end point of calcination was relatively advanced or delayed.

3.3. NIR Spectroscopy during Calamine Calcination. The near-infrared spectrum of calamine calcination could be grouped into three regions:

(1) The spectra in the 12500–7500 cm^{-1} region: The divalent cations of Ca, Fe, Cu, Cd, and Zn played an important role in determining the band positions in this spectral region [7]. These ions also caused shifts for the carbonate bands. Because the sample contained less impurity cations, the absorption characteristics in spectra were not significant.

(2) The spectra in the 7500–5750 cm^{-1} region, which were due to first overtones of the fundamental hydroxyl stretching modes and combination modes of OH stretching and bending modes [21]. All samples had absorption peaks at 7031 cm^{-1} and 6672 cm^{-1}. The absorption peak at 6672 cm^{-1} was related to OH in the structure of hydrozincite, and the hydrozincite was continuously decomposed into ZnO, CO_2, and H_2O during calcination [16]; the intensity of the absorption peak gradually weakened until it disappeared. The absorption peak at 7031 cm^{-1} was related to Zn–OH, while the peak shape was affected

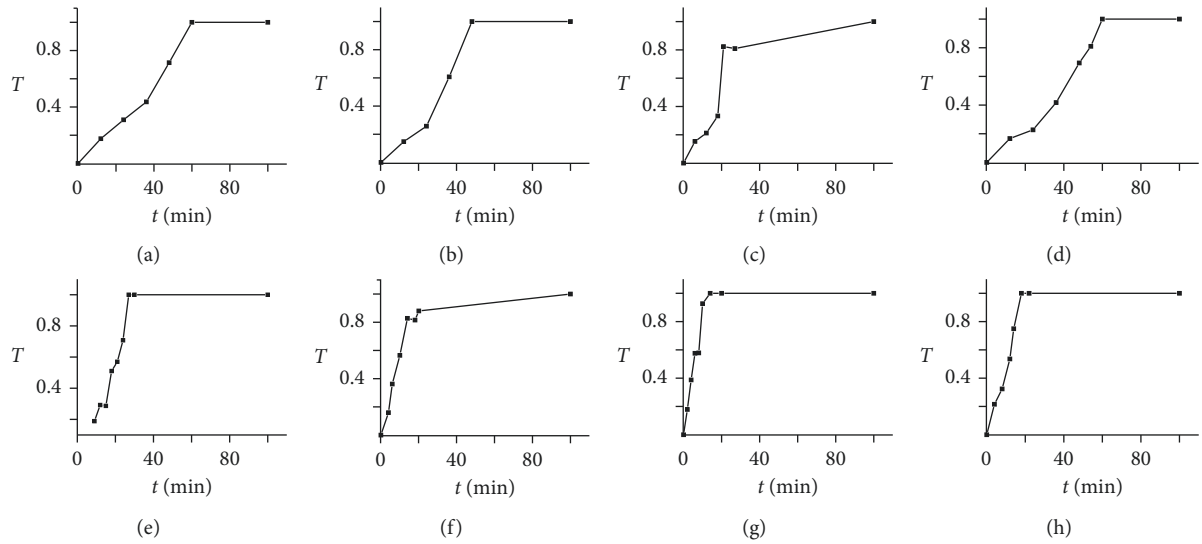

Figure 3: Change of XRD characteristic T value of 8 batches of calamine samples during calcination. (a) S1. (b) S2. (c) S3. (d) S4. (e) S5. (f) S6. (g) S7. (h) S8.

by impurities of the hemimorphite [$Zn_4(Si_2O_7)(OH)_2$]. For example, the samples S1, S3, S4, S5, S7, and S8 contained hemimorphite impurities, and the peak shape at 7031 cm^{-1} gradually became sharper with the increase of the relative content and crystallinity of the hemimorphite [22]. In contrast, samples S2 and S6 did not contain hemimorphite impurities, and the peak shape at 7031 cm^{-1} remained unchanged during calcination. The NIR spectrum of 8 batches of calamine samples during calcination in the 7500–5750 cm^{-1} region is shown in Figure 4.

(3) The spectra in the 5750–4000 cm^{-1} region were due to water and the carbonate ions [8]. The absorption feature in the range 5300–4900 cm^{-1} was the contribution of water-OH overtones, and the peak shape was affected by the impurity of hemimorphite. Samples S2 and S6 did not contain hemimorphite, the characteristic absorption of absorbed water was near 5082 cm^{-1} and 4919 cm^{-1}, and the peak shape was slow. Samples S1, S3, S4, S5, S7, and S8 contained hemimorphite, the characteristic absorption of adsorbed water was near 5215 cm^{-1}, 5059 cm^{-1}, and 4934 cm^{-1}, and the peak shape at 5215 cm^{-1} gradually became sharp during calcination. The characteristic of carbonate ion in hydrozincite was near 4349 cm^{-1} and 4170 cm^{-1}; during the calcination process, the intensity of the absorption peak gradually weakened until it disappeared. However, since there were carbonate impurities in some samples, a weak carbonate ion absorption peak would still appear after the hydrozincite was completely decomposed. For example, samples S5 and S7 contained some dolomite and calcite impurities, and after the hydrozincite was completely calcined, the carbonate ion absorption peaks [23] were seen at 4529 cm^{-1}, 4428 cm^{-1} and 4303 cm^{-1}. While the samples S3 and S4 contained dolomite impurities, the amount was very small, so the carbonate ion absorption peak was not obvious. The NIR spectrum of 8 batches of calamine samples during calcination in the 5750–4000 cm^{-1} region is shown in Figure 5.

The above had summarized to the contribution of NIR spectroscopy regions and change rules of absorption peaks during calamine calcination. The characteristic peaks of carbonate ion of hydrozincite were 4349 cm^{-1} and 4170 cm^{-1}; theoretically, both absorption peaks would disappear after the hydrozincite was completely decomposed. However, if the sample contained carbonate impurities, there would still be absorption peak near 4349 cm^{-1} after hydrozincite decomposition. So, the presence or absence of an absorption peak at 4170 cm^{-1} in the spectra could be used for judging the degree of calamine calcination.

3.4. NIR Model of Determining ZnO Content in Calcined Calamine. Information of sample classification is shown in Table 2. The NIR models determining the ZnO content of calcined calamine by different modeling parameters are shown in Table 3. From Table 3, it could be seen that model 1 had the smallest RMSECV value, and from the results of the validation set, there was no significant difference between models 1 and 2, and it was obviously better than other models. Therefore, it was determined that the modeling spectral band was 4601.6–4003.7 cm^{-1}, and the pretreatment method adopted SD. Besides, according to the RMSECV-rank correlation diagram (Figure 6(a)), when the RMSECV was the smallest, the best rank value of the model was determined to be 8. In addition, from the results of the prediction set, the RMSEP value of model 1 was the smallest, indicating the strongest predictability. The prediction results of the model for the training set, validation set, and test set are shown in Figures 6(b)–6(d).

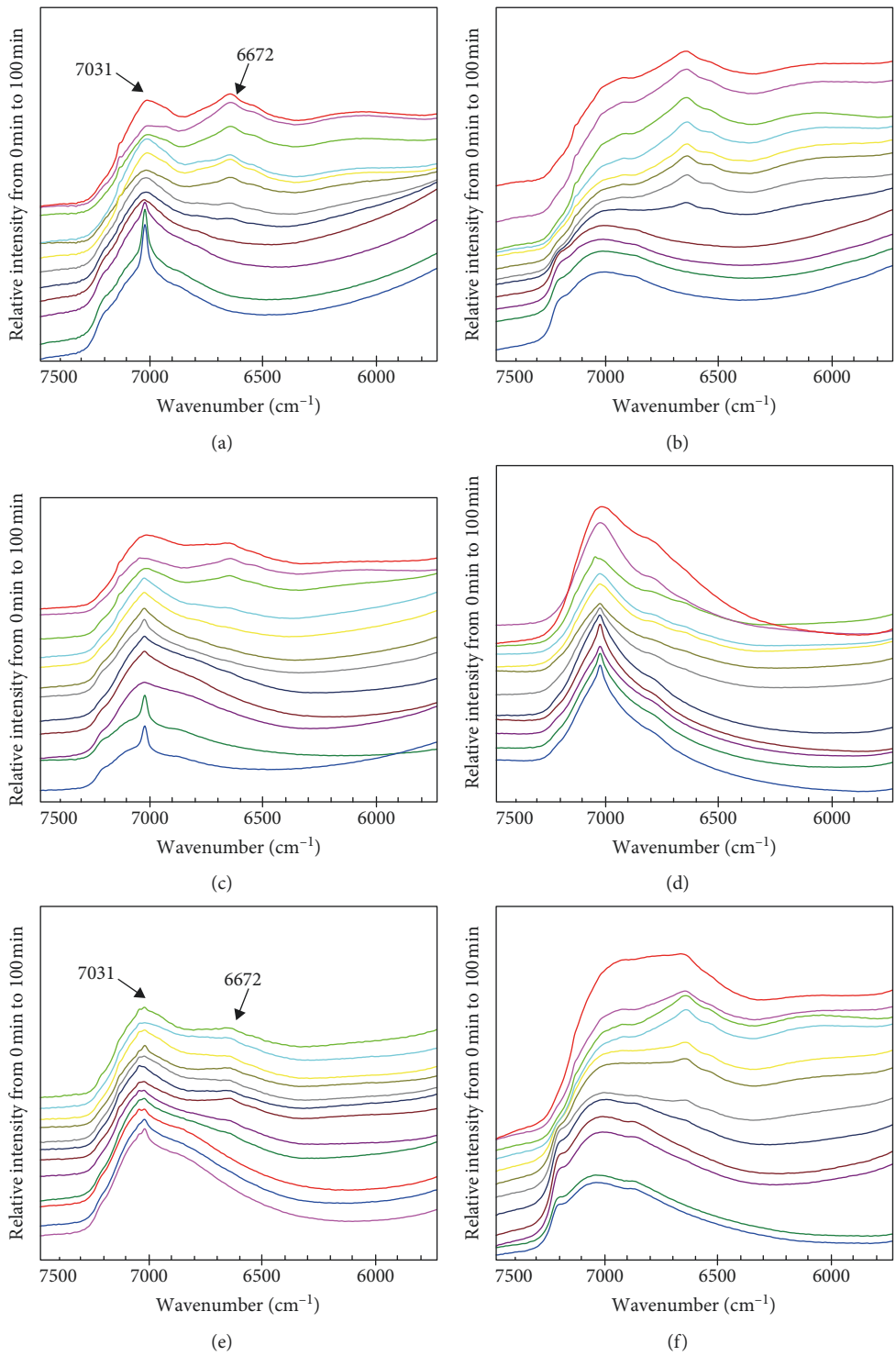

Figure 4: Continued.

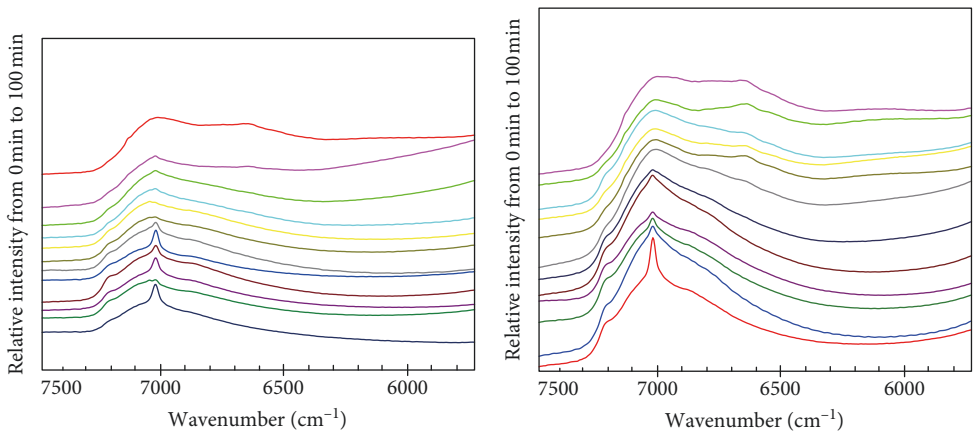

Figure 4: NIR spectra of 8 batches of calamine samples during calcination in the 7500–5750 cm^{-1} region. (a) S1 (hydrozincite and hemimorphite). (b) S2 (hydrozincite). (c) S3 (hydrozincite, hemimorphite, and dolomite). (d) S4 (hydrozincite, hemimorphite, and dolomite). (e) S5 (hydrozincite, hemimorphite, dolomite, and calcite). (f) S6 (hydrozincite). (g) S7 (hydrozincite, hemimorphite, dolomite, and calcite). (h) S8 (hydrozincite and hemimorphite).

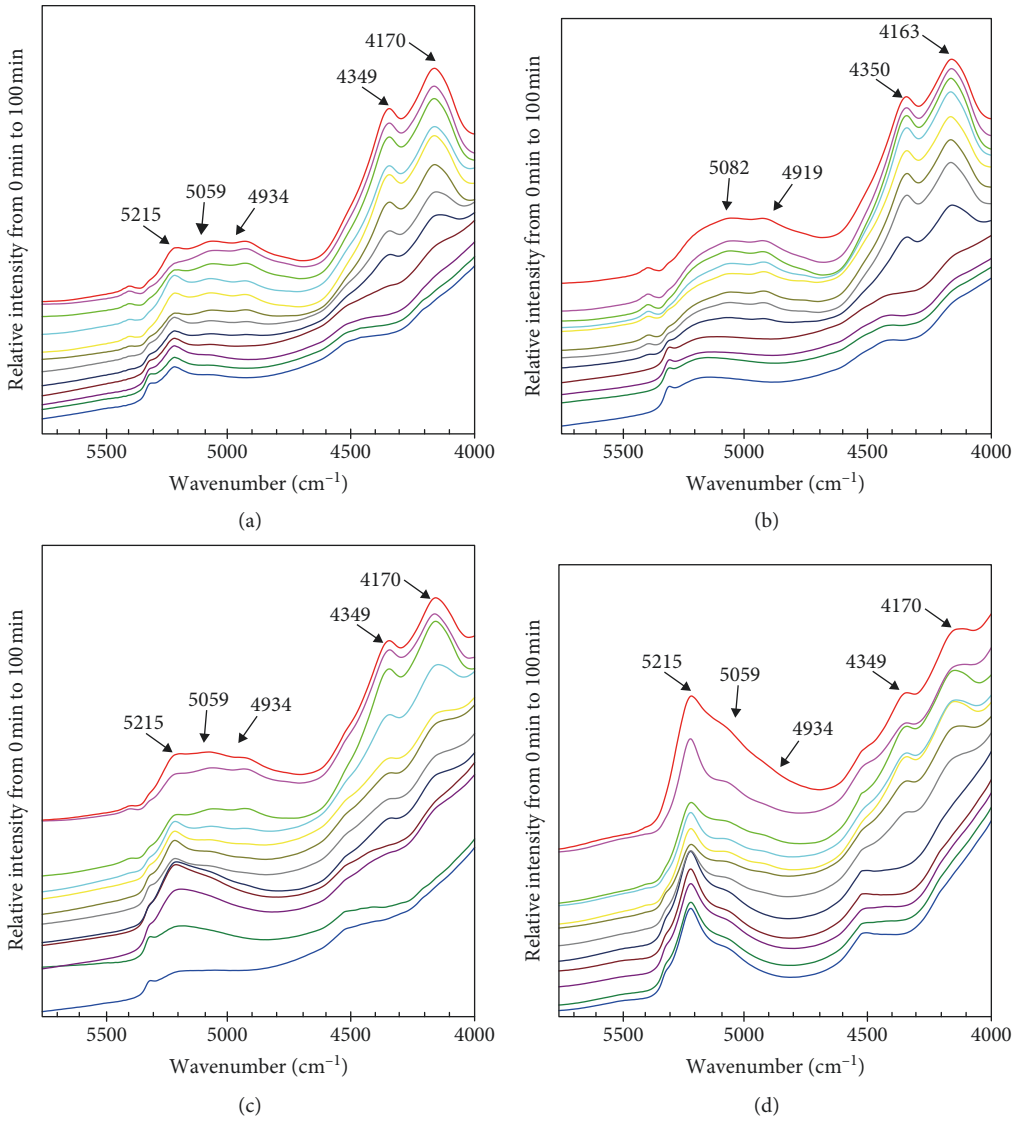

Figure 5: Continued.

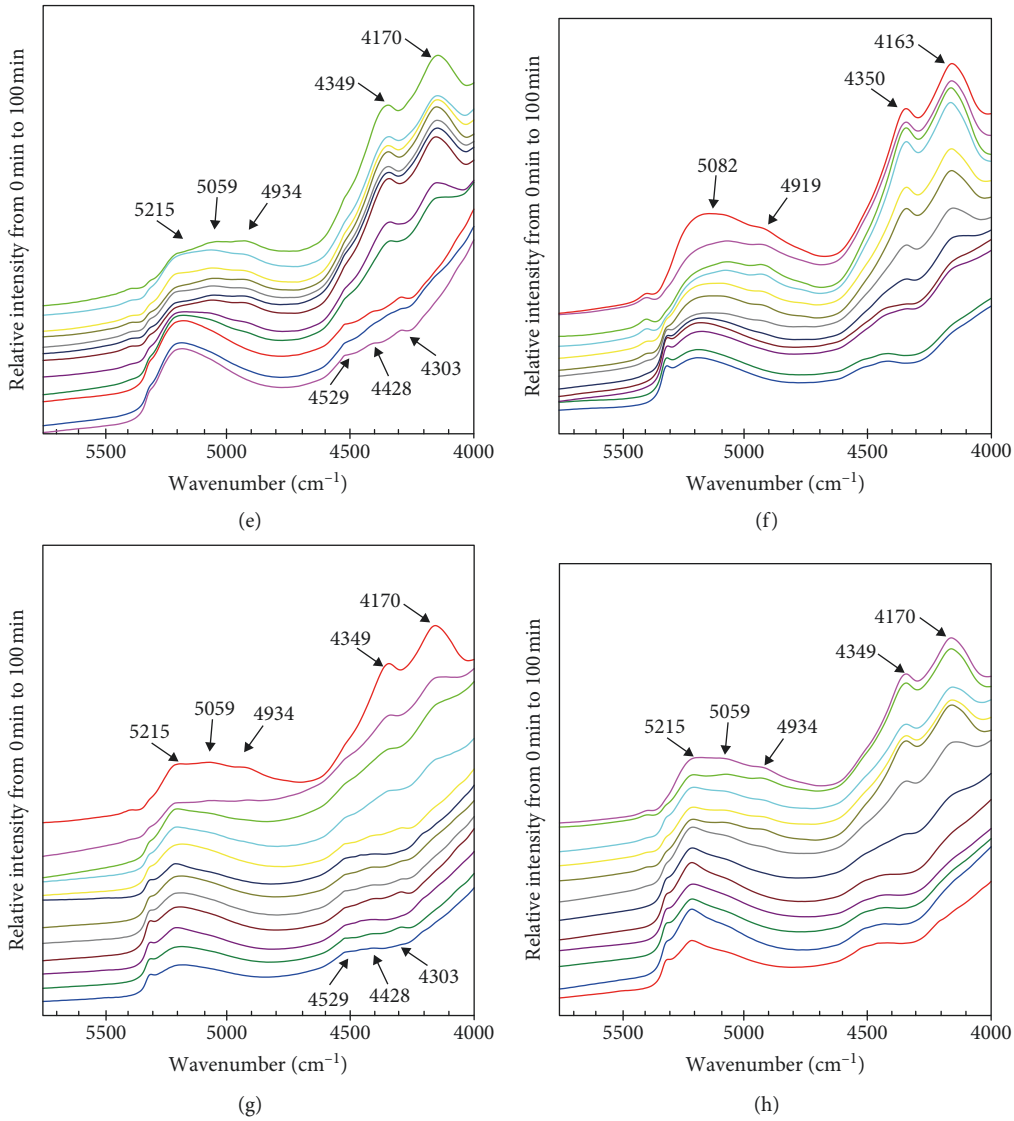

Figure 5: NIR spectra of 8 batches of calamine samples during calcination in the 5750–4000 cm^{-1} region. (a) S1 (hydrozincite and hemimorphite). (b) S2 (hydrozincite). (c) S3 (hydrozincite, hemimorphite, and dolomite). (d) S4 (hydrozincite, hemimorphite, and dolomite). (e) S5 (hydrozincite, hemimorphite, dolomite, and calcite). (f) S6 (hydrozincite). (g) S7 (hydrozincite, hemimorphite, dolomite, and calcite). (h) S8 (hydrozincite and hemimorphite).

Table 2: Information of sample classification.

Set	Number of samples	Minimum (%)	Maximum (%)	Average value (%)	SD (%)
Training	73	43.43	93.43	73.84	12.36
Validation	32	49.43	93.34	72.47	13.70
Test	25	45.69	93.21	74.51	12.18

Table 3: NIR models for determining ZnO content in calcined calamine.

Model	Spectral band (cm^{-1})	Pretreatment	RMSECV (%)	Validation set			Test set			Rank
				R^2 (%)	RMSEV (%)	RPD	R^2 (%)	RMSEP (%)	RPD	
1	4601.6–4003.7	SD	2.81	94.93	3.09	4.52	97.75	1.89	6.44	8
2	5446.3–4003.7	SD	2.9	94.96	3.08	4.62	95.75	2.79	4.36	8
3	7436.5–5778, 4601.6–4003.7	SD	2.97	94.74	3.14	4.41	97.69	1.97	6.18	8
4	7436.5–5778, 5446.3–4003.7	SD	3.01	94.57	3.19	4.42	93.87	3.19	3.82	8
5	7436.5–5778, 5446.3–4003.7	NO	3.09	93.20	3.57	3.89	90.52	4.28	2.85	8
6	7436.5–5778, 5446.3–4003.7	FD	3.14	93.92	3.38	4.14	94.99	2.97	4.11	8

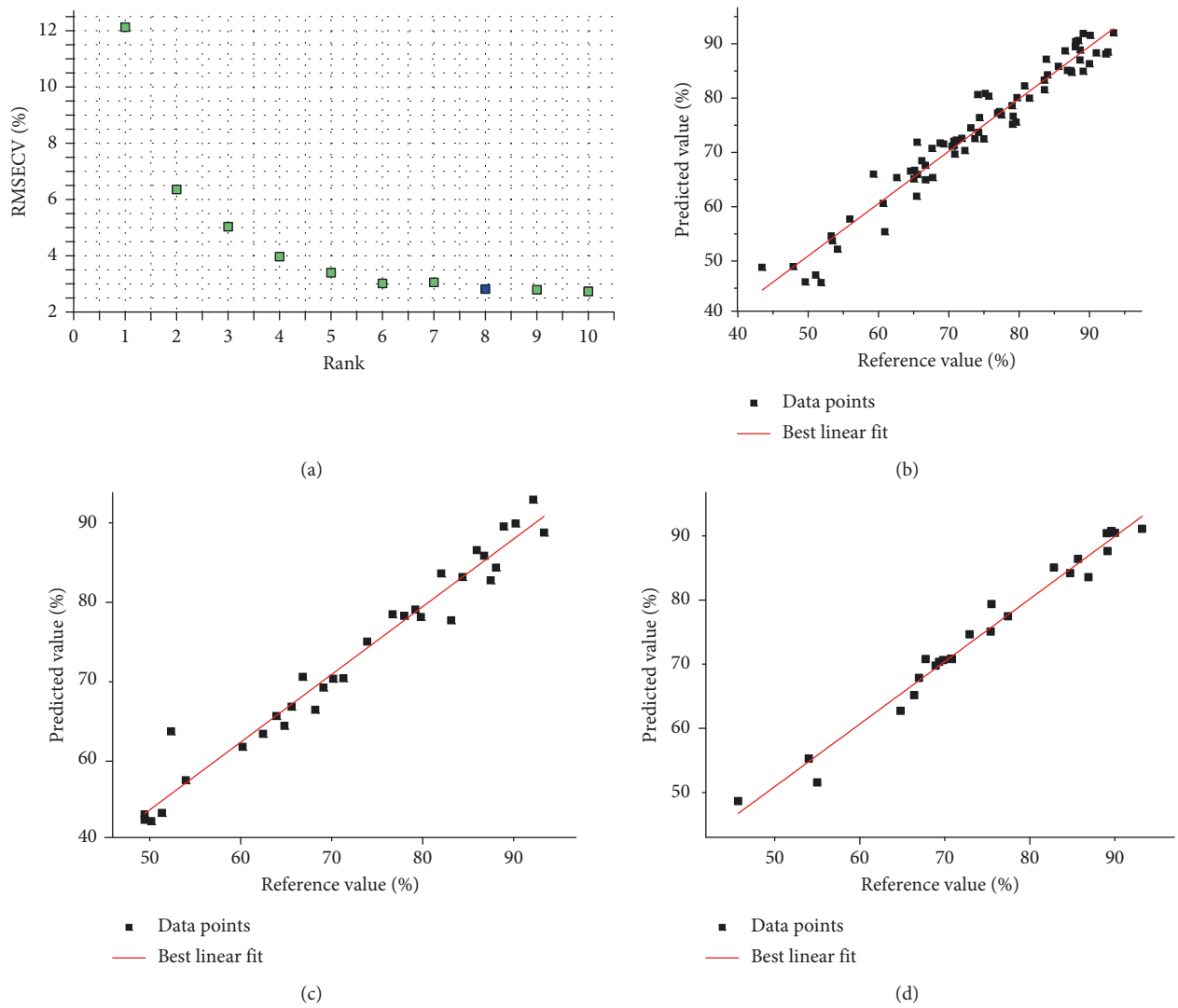

FIGURE 6: RMSECV-rank correlation diagram (a) and the prediction results of the model for the training set (b), validation set (c), and test set (d).

In terms of the internal cross-validation, the RMSECV was 2.81%. In the predicted results of validation set, the RMSEV was 3.09%, the R^2 was 94.93%, and the RPD was 4.52. In the predicted results of test set, the RMSEP was 1.89%, the R^2 was 97.75%, and the RPD was 6.44. It indicated that the prediction accuracy of the model was fine.

3.5. NIR Model for Predicting the XRD Characteristic T Value. The NIR models for predicting the XRD characteristic T value by different modeling parameters are shown in Table 4. From Table 4, it could be seen that model 1 had the smallest RMSECV value. In the external validation, the RMSEP value of model 1 had no significant difference with the minimum of 0.0813%, and model 1 was finally determined to be the best model. According to the RMSECV-rank correlation diagram (Figure 7(a)), when the RMSECV was the minimum, the best rank value of the determined model was 10. The prediction results of the model for the training set and prediction set are shown in Figure 7(c). The model was excellent with RMSECV of 0.0721%, R^2 of 96.01%, and RPD of 5.01 in internal cross-validation and RMSEP of 0.0829%, R^2 of 94.95%, and RPD of 4.64 in external validation. The predicted values of prediction set samples are shown in Table 5.

When the T value was equal to 1, the calamine was completely calcined. However, from the results of Table 5, it could be seen that there was a deviation between the T value predicted by the NIR model and its reference value. Samples whose reference value of T was 1, numbered 1, 10, 28, 37, and 46, were selected and the average of their relative deviations was calculated to be 4.08%. In addition, taking into account some errors in the experimental analysis process, this study stipulated that the calamine calcination was completed when the T value was $1.00 \pm 5\%$.

4. Conclusions

In the earlier stage, our research group established a rapid identification model for calamine and a determination model of ZnO content in calamine by near-infrared spectroscopy [3, 4]. However, the clinical use of calamine

Table 4: NIR models for predicting characteristic T value of XRD pattern.

Model	Spectral band (cm^{-1})	Pretreatment	Internal cross-validation			External validation			Rank
			R^2 (%)	RMSECV (%)	RPD	R^2 (%)	RMSEP (%)	RPD	
1	7436.6–5778, 4601.6–3999.9	SNV	96.01	0.0721	5.01	94.95	0.0829	4.64	10
2	5446.3–3999.9	MSC	94.53	0.0844	4.28	90.26	0.1150	3.51	9
3	7436.6–5778, 5446.3–3999.9	SNV	94.49	0.0848	4.26	95.15	0.0813	5.23	9
4	7436.6–6607.3, 4601.6–3999.9	SNV	93.44	0.0924	3.91	92.36	0.1020	3.9	8
5	6607.3–5778, 4601.6–4300.7	SNV	93.35	0.0931	3.88	93.12	0.0968	3.96	6
6	5446.3–3999.9	SNV	93.28	0.0936	3.89	90.83	0.1120	3.62	9

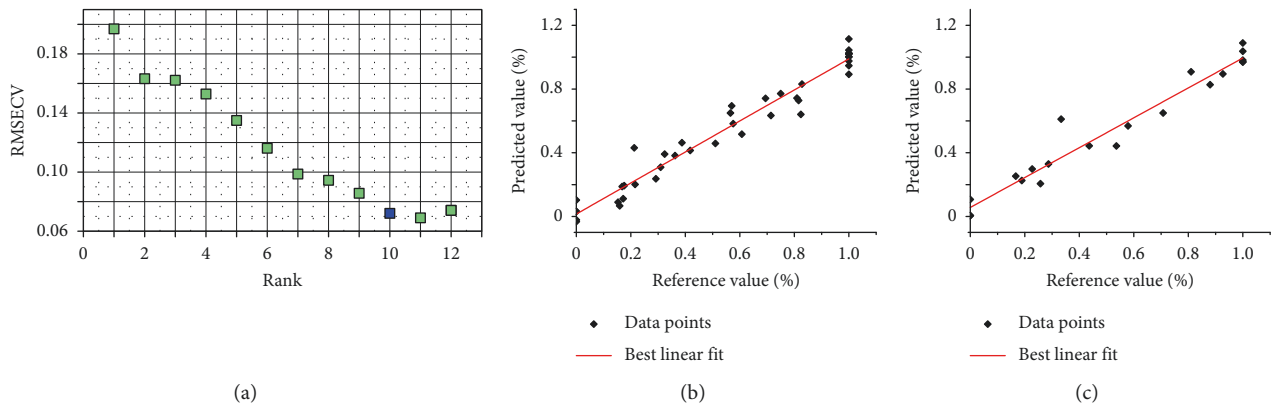

(a) (b) (c)

Figure 7: RMSECV-rank correlation diagram (a) and the prediction results of the model for the training set (b) and prediction set (c).

Table 5: Predicted T values of prediction set samples.

Number	Reference value (%)	Predicted value (%)	Deviation (%)	Relative deviation (%)
1	1.0000	1.0887	−0.0887	8.87
4	0	0.0054	−0.0054	∞
7	0.4364	0.4433	−0.0069	1.58
10	1.0000	0.9705	0.0295	2.95
13	0.1667	0.2530	−0.0863	51.77
16	0.8099	0.9086	−0.0987	12.19
19	0.2273	0.2976	−0.0703	30.93
22	0	0.1065	−0.1060	∞
25	0.3331	0.6114	−0.2780	83.46
28	1.0000	1.0370	−0.0370	3.7
31	0.2573	0.2056	0.0517	20.09
34	0.5359	0.4426	0.0933	17.41
37	1.000	0.9816	0.0184	1.84
40	0.5786	0.5687	0.0099	1.71
43	0.9268	0.8948	0.0320	3.45
46	1.0000	0.9696	0.0304	3.04
49	0.8800	0.8275	0.0525	5.97
52	0.1887	0.226	−0.0373	19.77
55	0.2867	0.3292	−0.0425	14.82
58	0.7076	0.6495	0.0581	8.21
61	0	0.0054	−0.0054	∞

required calcination, and currently, there was no good way to monitor the process of calamine calcination online. In this study, the calcination process of 8 batches of calamine samples with different sizes and textures under different calcination temperatures was simulated, to analysis the change rules of ZnO contents, XRD patterns of samples, and the attribution of absorption regions in near-infrared spectra. In the calcination process of calamine, the content of ZnO gradually increased to the maximum and then remained unchanged; at that time, the calamine was completely calcined. The XRD characteristic T value could be used to measure the degree of decomposition of hydrozincite into ZnO. When the T value was 1, the hydrozincite was completely decomposed into ZnO, that is, the calamine was

completely calcined. In near-infrared spectroscopy analysis, the absorption of carbonate ion in hydrozincite was $4349\,m^{-1}$ and $4170\,cm^{-1}$, and the absorption peak of $4170\,cm^{-1}$ was not interfered by other carbonic impurities, which would disappear when the calamine was completely calcined.

In addition, this paper established a rapid determination model of ZnO content in calcined calamine using near-infrared spectroscopy based on the PLS algorithm. It was found that the model enjoyed a high accuracy and strong forecasting capacity for analyzing ZnO content ranging within 41.13–93.43%. That is, from the content point of view, the quality of the calcined calamine and the calcination process could be monitored throughout by NIR without titration of ZnO.

This paper also established a NIR model for predicting T value. When applied, the near-infrared spectrum of the sample was brought into the model to obtain the T value. If the T value was $1.00 \pm 5\%$, the sample was completely calcined. This method not only can judge the end point of the calamine calcination process but also can judge the calcination degree of any calamine sample. It had the outstanding advantages of rapidness, environmental protection, and no need to process samples, compared with measuring the change of the ZnO content in the calamine calcination. It was of great significance to optimize the calcination technology of calamine and monitor the quality of calamine processed in actual production.

Data Availability

The data used to support the findings of this study are included within the article.

Conflicts of Interest

The authors declare that there are no conflicts of interest regarding the publication of this paper.

Acknowledgments

This work was supported by the high-technology projects of the National Development and Reform Commission (1399), "Standardized Construction of Musk Hemorrhoids Ointment."

References

[1] National Pharmacopoeia Committee, *China Pharmacopoeia of 2015 Edition,* Vol. 1, China Medical Science and Technology Press, Beijing, China, 2015.

[2] L. J. Yang, Z. J. Zhang, R. R. Li, S. Q. Sun, and R. C. Lin, "Study on the mineralogical origin of medicinal calamine based on phase and composition analysis," *Guang Pu Xue Yu Guang Pu Fen Xi*, vol. 31, no. 11, pp. 3092–3097, 2011.

[3] Y. Sun, L. Chen, B. Huang, and K. Chen, "A rapid identification method for calamine using near-infrared spectroscopy based on multi-reference correlation coefficient method and back propagation artificial neural network," *Applied Spectroscopy*, vol. 71, no. 7, pp. 1447–1456, 2017.

[4] X. Zhang, L. Chen, Y. Sun, Y. Bai, B. Huang, and K. Chen, "Determination of zinc oxide content of mineral medicine calamine using near-infrared spectroscopy based on MIV and BP-ANN algorithm," *Spectrochimica Acta Part A: Molecular and Biomolecular Spectroscopy*, vol. 193, pp. 133–140, 2018.

[5] Y. M. Guo, K. F. Yu, Y. H. Liu, J. Z. Zhao, Z. C. Wang, and H. B. Zhang, "Analysis on processing mechanism of calamine," *Zhongguo Zhongyao Zazhi*, vol. 30, no. 8, pp. 596–599, 2005.

[6] L. Zhou, C. Xu, L. Zhang, and A. Ding, "Processing mechanism of calamine," *Zhongguo Zhongyao Zazhi*, vol. 35, no. 12, pp. 1556–1559, 2010.

[7] F. J. Camino-Sánchez, B. Delgado-Moreno, and P. Navarro-Fuentes, "Quick development of a NIRS method for the analysis of moisture, protein, and fat in nutritional clinical products," *Food Analytical Methods*, vol. 8, no. 7, pp. 1758–1770, 2015.

[8] R. L. Frost, B. J. Reddy, M. C. Hales, and D. L. Wain, "Near infrared spectroscopy of the smithsonite minerals," *Journal of Near Infrared Spectroscopy*, vol. 16, no. 2, pp. 75–82, 2008.

[9] K. L. Chen and L. Chen, "Identification methods on mineral traditional Chinese medicines by near infrared (NIRS) spectroscopy technology," *Zhongnan Minzu Daxue Xuebao*, vol. 33, no. 4, pp. 52–56, 2014.

[10] C. W. Huck, G. Abel, M. Popp, and G. K. Bonn, "Comparative analysis of naphthodianthrone and phloroglucine derivatives in St. John's Wort extracts by near infrared spectroscopy, high-performance liquid chromatography and capillary electrophoresis," *Analytica Chimica Acta*, vol. 580, no. 2, pp. 223–230, 2006.

[11] L. Xiang, G. Fan, J. Li et al., "The application of an artificial neural network in the identification of medicinal rhubarbs by near-infrared spectroscopy," *Phytochemical Analysis*, vol. 13, no. 5, pp. 272–276, 2010.

[12] Y. Chen, M. Y. Xie, Y. Yan et al., "Discrimination of Ganoderma lucidum according to geographical origin with near infrared diffuse reflectance spectroscopy and pattern recognition techniques," *Analytica Chimica Acta*, vol. 618, no. 2, pp. 121–130, 2008.

[13] L. Ye, K. Li, W. Wang, Y. Liu, S. Jiang, and G. Huang, "Near-infrared spectroscopy as a process analytical technology tool for monitoring the parching process of traditional Chinese medicine based on two kinds of chemical indicators," *Pharmacognosy Magazine*, vol. 13, no. 50, pp. 332–337, 2017.

[14] C. B. Luo, L. W. Chen, Y. L. Yan, W. Z. Wang, and Z. Y. Wang, "Study of temperature correction in the PLS near-infrared quantitative analysis of the wheat," *Guang Pu Xue Yu Guang Pu Fen Xi*, vol. 27, no. 10, pp. 1993–1996, 2007.

[15] Z. L. Wang, Y. Bai, J. T. Ding, and F. W. Ning, "Analysis method of mica content of artificial aggregate based on X-ray diffraction," *Shuidian Nengyuan Kexue*, vol. 35, no. 3, pp. 150–153, 2017.

[16] J. H. Zhang, X. J. Shi, Z. Wei, L. Yin, and Y. P. Liu, "Component analysis and thermal stability of calamine before and after processing," *Zhongguo Shiyan Fangjixue Zazhi*, vol. 17, no. 24, pp. 16–18, 2011.

[17] Z. Ni, C. Hu, and F. Feng, "Progress and effect of spectral data pretreatment in NIR analytical technique," *Yaowu Fenxi Zazhi*, vol. 28, no. 5, pp. 824–828, 2008.

[18] H. H. Zhao and Y. L. Yan, "The effects of noise on NIR analysis and related mathematic pretreatments and models," *Guangpuxue Yu Guangpu Fenxi*, vol. 26, no. 5, pp. 842–845, 2006.

[19] B. K. Waruru, K. D. Shepherd, G. M. Ndegwa, P. T. Kamoni, and A. M. Sila, "Rapid estimation of soil engineering properties using diffuse reflectance near infrared spectroscopy," *Biosystems Engineering*, vol. 121, no. 18, pp. 177–185, 2014.

[20] V. Bellon-Maurel, E. Fernandez-Ahumada, B. Palagos, J. M. Roger, and A. McBratney, "Critical review of chemometric indicators commonly used for assessing the quality of the prediction of soil attributes by NIR spectroscopy," *TrAC Trends in Analytical Chemistry*, vol. 29, no. 9, pp. 1073–1081, 2010.

[21] B. J. Reddy and R. L. Frost, "Near infrared spectroscopy of aurichalcite $(Zn,Cu^{2+})_5(CO_3)_2(OH)_6$," *Journal of Near Infrared Spectroscopy*, vol. 15, no. 2, pp. 115–121, 2007.

[22] L. Chen, M. Y. Yuan, and K. L. Chen, "Induction and analysis for NIR features of frequently-used mineral traditional Chinese medicines," *Zhongguo Zhongyao Zazhi*, vol. 41, no. 19, pp. 3528–3536, 2016.

[23] R. L. Frost, B. J. Reddy, D. L. Wain, and M. C. Hales, "An application of near infrared spectroscopy to the study of carbonate minerals-smithsonite, rhodochrosite, sphaerocobaltite and cadmium smithsonite," *Journal of Near Infrared Spectroscopy*, vol. 14, no. 5, pp. 317–324, 2006.